Orbit Determination of 1972 XA via the Gaussian method

Annie Polish, Malick Sere, & Lucy Zhu

SSP 2016, New Mexico Tech

July 23, 2016

Near Earth Asteroids, or NEAs, can be a threat to the Earth, due to their location between the orbits of Mars and Venus. With four sets of images taken during June and July 2016, we determine the α and δ of a near earth asteroid *1866 Sisyphus* using Least Squares Plate Reduction. We then use this data and Gauss's method of orbit determination to calculate the orbital elements. We compare several strategies for determining and refining the orbital elements within the method of Gauss. These elements are checked against JPL HORIZONS data, and found to be accurate to within 0.001AU or 0.06°. Furthermore, they are used to predict the observations of another group working on the same asteroid, which they successfully predict to within 2% error.

1. Introduction

A Near Earth Asteroid (NEA) is an asteroid with an orbit that at least partially lies between 0.9AU and 1.3AU. These objects are extremely abundant in the solar system, and many of them are large enough to pose a serious threat to the earth. We investigate the orbit of *1866 Sisyphus*, which measures approximately 8 km in diameter, making it one of the largest NEAs. Data was collected using a Celestron C-14 at New Mexico Tech's Etscorn Observatory, during 4 nights spanned over June and July 2016.

We use data reduction software to remove thermal noise, electronic noise, and dust from the CCD images. Astrometric data is extracted from the images using Least Squares Plate Reduction (LSPR). Using the method of Gauss, the classical orbital elements are determined from the positional data. These elements are checked via comparison with established JPL HORIZONS values, and used to predict the location of *1866 Sisyphus* at future dates.

2. Materials and Methods

2.1. Observation Materials and Methods

Observations were taken on a 14-inch Schmidt-Cassegrain telescope with a focal length of 3910mm and a 356mm aperture, fitted with a 0.6x focal reducer. Images were recorded on a SBIG ST-10 CCD chip, with 2184x1472 pixels, each 6.8μm on a side, with an angular size of 0.6 arcseconds. 2x2 binning was used for every image. The CCD was cooled using a thermocouple to -5°C to reduce thermal noise. For each night of images, a set of bias (electronic noise) images and dark current images were also taken, for use in data reduction.

Ephemeridies for each night's observations were produced using JPL HORIZONS. TheSkyX virtual planetarium software was used to generate star charts, locate bright stars to focus the telescope on, and control the telescope itself. After images were captured, they were reduced in CCDsoft, to remove the noise indicated by our dark and bias images. CCDsoft was also used to align images from multiple sets, so that they could be easily compared to locate the asteroid.

Python 2.7.11, with NumPy and AstroPy, was used to conduct photometry and astrometry on each images.

2.2. Observations

Table 1: Observation Data

Date	**Exp. Time**	**Num. Images**	**CCD Temp.**	**Conditions**
June 22	300s	10	-2°C	Bright moon
July 4	120s	20	-5°C	Dark and clear
July 12	120s	15	-5°C	Clear sky
July 21	200s	3	-5°C	Cloudy

All observations were taken using a visual filter, with the telescope focused to the appropriate setting using the focusing grid and the respective night's focus star. All sets of images were taken between 3:00 and 5:00 UTC.

2.3. The Method of Gauss

The orbit of *1866 Sisyphus* was determined using the method of Gauss, a combination of Keplers 3rd Law and the Law of Universal Gravitation, initially invented by Gauss to determine the orbit of Ceres. Given three sets of α, δ, and Julian dates for *1866 Sisyphus*, we utilized the method to calculate two dates position and velocity vectors in order to find the middle dates position and velocity vectors in ecliptic rectangular coordinates.

The general goal of the method of Gauss is a simple vector calculation, $\vec{r} = \rho\hat{\rho} - \vec{R}$, where $\vec{R}$ is the vector from the earth to the sun, $\hat{\rho}$ is the unit vector or direction from earth to the asteroid, and ρ is the distance from the earth to the asteroid. Simple calculations yield $\hat{\rho}$ from α and δ while $\vec{R}$ can be looked up using JPL HORIZONS. The core problem is to find ρ, the range to the asteroid. An initial guess for the distance from the asteroid to the sun is found using the scalar equations of range and the scalar equation of Lagrange. Then, the initial guess is improved iteratively, using either a 4th order Taylor series or closed-form functions. On each iteration, the recalculated values are entered back in to the scalar equations of Lagrange, to produce another ρ guess to put back into the vector calculation

Once we determined the second observations position and velocity vector from the method of Gauss, the asteroids six main orbital elements: semi-major axis (a), eccentricity (e), argument of perihelion (ω), inclination (i), longitude of ascending node (Ω), and mean anomaly (M) were calculated and later plugged into Visual Python to generate a physical representation of the asteroid's orbit (see Table 1)

2.4. Additional Methods

We used two different implementations of the method of Gauss to compute our orbital elements. Two of us used closed-form f and g functions, and one used a truncated Taylor series. In general, closed form functions performed significantly better than the truncated Taylor series. The orbital elements calculated with the Taylor series were roughly correct, but had much larger uncertainties; up to two orders of magnitude larger than that of the closed form functions. As an additional test of the orbital elements, we visualized the asteroid's orbit relative to those of Earth and Mars. (1)

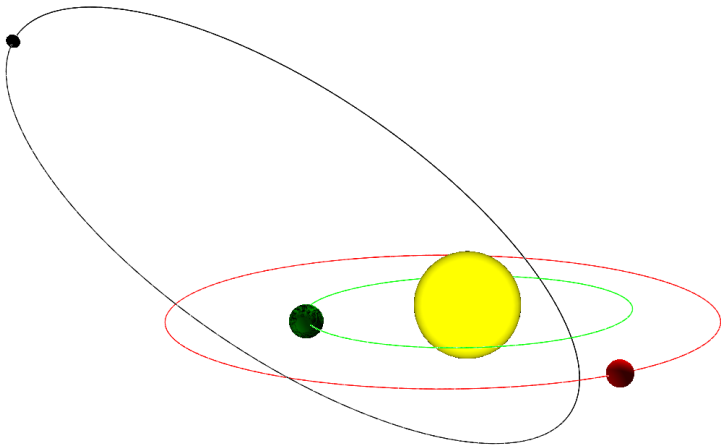

Figure 1: The orbits of Earth, Mars, and *1866 Sisyphus* simulated in vPython

3. Data and Analysis

3.1. Observational Data

Table 2: Calculated Coordinates

Date	α	α **uncert.**	δ	δ **uncert.**	**V Mag.**	**SNR**
June 22	$13_h36_m41.27_s$	0.34s	12°02′21.47”	0.32”	16.5	30
July 4	$13_h32_m24.21_s$	0.30s	08°24′15.97”	0.33”	16.5	32
July 12	$13_h32_m05.34_s$	0.35s	05°54′15.28”	0.30”	16.7	20
July 21	$13_h33_m54.39_s$	0.28s	03°02′50.18”	0.29”	16.4[1]	20

3.2. Data Reduction

After obtaining least three sets of five images during each observation night, we used CCDsoft to reduce the noise in the images by subtracting the bias and dark images we took during each observation night, as well as flats. The bias frames have zero exposure time, and measure electronic noise in the CCD and other hardware. The dark images are exposed with the shutter closed for the same length of time as the observation frames, and measure thermal electron noise on the CCD chip. The reduced images were then aligned, combined, and finally blinked on CCDsoft to allow us to visually identify the asteroid.

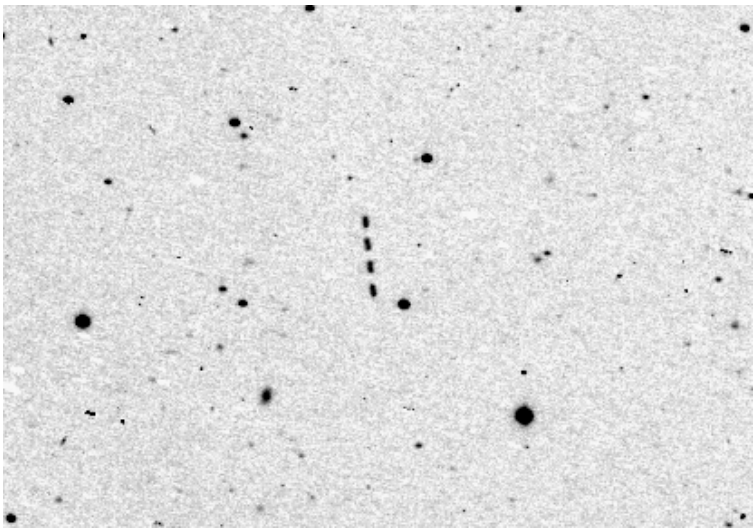

Figure 2: *1866 Sisyphus* in 4 flattened images on July 4th

With LSPR codes programmed in Python, we performed astrometry on the middle image of the middle set of images taken during observations. 12 reference stars were initially selected, and their sub-pixel coordinates were determined via centroiding, which finds the average sub-pixel location by averaging pixels weighted by brightness. The LSPR code fits a transformation between (x, y) pixel values and (α,δ) found using TheSkyX. Then, these transformation constants were used to map the coordinates of our asteroid into (α, δ). Each of the calculated values match ephemeris values to within one arcsecond. We also created a modification of out LSPR programs to account

[1] Clouds partially obscured the asteroid

for the curvature of the sky. This allowed us to more accurately calculate the right ascension and declination of our asteroid with a reference stars farther away. This was especially important with our particular asteroid, because it resides in a section of the sky with few stars. As a result, there were few good options for reference stars. It was difficult to create a circle around the asteroid and issues arose in attempts to keep the asteroid in a central location relative to the reference stars. With the flattening correction, we were able to achieve low uncertainties: the highest uncertainty in any of our right ascension or declination measurements was 0.35 arcseconds, and out uncertainties were as low as 0.27 arcseconds.

To obtain the magnitude of the asteroid, we conducted photometry by comparing the pixel brightness of our asteroid to that of five reference stars. The reference stars were selected according to their magnitude and proximity to other stars, since photometry is more accurate when it uses stars close to the predicted brightness of the target object. These stars were used to fit a linear equation to the relationship between pixel value and apparent magnitude, which could then be used to find the magnitude of an unknown object. All of the calculated magnitudes for *1866 Sisyphus* were within ±0.5 magnitude of the established JPL values, which is acceptable for such a simplistic photometry measurement.

We also modified our photometry programs to obtain signal to noise ratios and sky background values. Most of the required components to do this were already available in the photometry code. In order to calculate the sky brightness, we used the following equation: $-2.5 * log_{10}(signal) + c$ where the signal was the average sky pixel count of the annulus around our asteroid divided by the plate constant, 1.196 arcseconds per pixel, squared, in order to obtain ADU per arcsecond squared. In order to find the constant, c, we reversed the equation and used the asteroid's signal and its previously calculated magnitude. Inputting these values in our equation, we were able to obtain the apparent magnitude of the background sky in magnitudes per arcsecond squared.

After finding the sky brightness, we proceeded to calculate the SNR of the asteroid in our images. The signal was calculated in the same way as was calculated for photometry. to find dark current, we subtracted bias frames the that observation's dark frames, and use python to calculate the average pixel count. Using this, and the telscopes known gain of 1.3 e- per ADU, we were able to calculate the SNR for each of our observations

3.3. Orbital Elements

Table 3: Calculated Orbital Elements

Element	**A. Polish**	**M. Sere**	**L. Zhu**
a	1.8942AU±0.003	1.9116AU±0.03	1.8791AU±0.05
e	0.5389AU±0.004	0.5381AU±0.008	0.5395AU±0.0009
i	41.166°±0.03	40.323°±0.7	41.357°±1.5
ω	293.040°±0.04	293.636°±0.6	291.465°±5.9
Ω	63.523°±0.02	64.344°±0.7	63.795°±3.2
M	293.417°±2.2	293.954°±2.7	293.208°±7.7

Orbital elements describe the physical properties of orbiting objects such as the asteroid. The semi-major axis, a, is the average distance between the asteroid and the sun. Eccentricity, e, measures how far off the orbit is from circular, and ranges from 0 to 1. Inclination, i, is the angle between the plane of the orbit and the plane of the ecliptic. The argument of perihelion (ω) and longitude of ascending node (Ω) angularly orient the orbit with respect to the ecliptic, as shown in Fig. 3. Finally, the mean anomaly M pinpoints the location of the asteroid within its orbit at a

given time, in this case 9:00 MDT on June 27th, 2016.

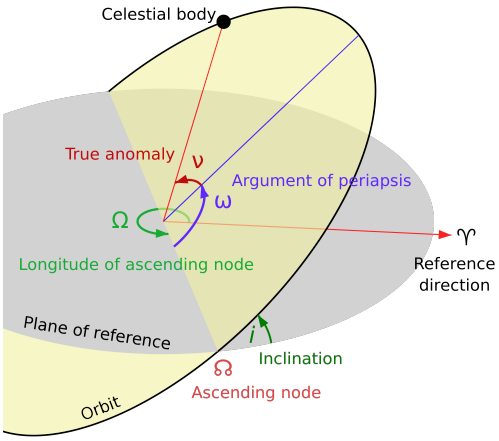

Figure 3: Orbital elements[2]

Based on a and e, it is trivial to compute the perihelion of *1866 Sisyphus*, which is approximately 0.9AU. This means it is categorized as an Earth Crosser, because its perihelion is within the orbit of the Earth. In addition, its semi-major axis is larger than that of Earth, making it an Apollo asteroid.

3.4. Testing the Orbital Elements

Due to the presence of four sets of observations (where Gauss's method needs only three), we were able to use the JackKnife method to compute uncertainties on the orbital elements by comparing the results of the four possible combinations of observations. For each orbital element, we first found the average value, and from that calculated the RMS value of the combined four observations. Using the most accurate orbital element (of the 3 sets we produced), all 6 of our orbital elements match the established JPL values for our asteroid to within the calculated uncertainties.

We also tested our model of the asteroid's orbit by using the orbital elements to predict the position of the asteroid at the times when Team 10 was observing it. We predicted its angular position in the sky to within 2% for each observation, proving that our orbital elements are accurate enough to be useful for projecting into the past or predicting the future of our asteroid.

Table 4: Predicting the position of *1866 Sisyphus*

Day and Coordinate	Observed	Calculated	Percent Error
July 7th, α	$13_h32_m35_s$	$13_h32_m45_s$	0.07%
July 7th, δ	08°42′43”	08°08′32”	−2.0%
July 11th, α	$13_h32_m02_s$	$13_h32_m11_s$	0.07%
July 11th, δ	06°12′34”	06°05′53”	−1.8%
July 15th, α	$13_h32_m27_s$	$13_h32_m29_s$	$< 0.01\%$
July 15th, δ	04°56′43”	04°56′09”	−0.2%

[2]Wikimedia Commons

3.5. Differential Correction

Differential correction is a method to improve orbit determination. It uses a $6x6$ Jacobian matrix to compute the optimal change in each of the 6 elements of the $\vec{r}$ and $\dot{\vec{r}}$ vectors to reduce the error in those vectors. It requires more than three observations, which theoretically allows us to take advantage of any extra data we gather. Each of us programmed differential corrections, but none of them improved the orbital elements. In one implementation, the calculated changes were subtracted instead of added, which actually improved the values more than when they were added, producing an RMS value of 0.001 rather than 0.005. In another implementation, three orbital elements improved, but the other three got worse, and the overall $O - C$ value was higher. Rather than yielding improved position and velocity vectors and subsequently improved orbital elements, the differential correction outputted values with higher deviation from those given by JPL HORIZONS. For our final orbital elements, we decided not to use differential corrections, because it was too inconsistent to reliably improve our data.

4. Conclusion

As the established JPL's values falls within the measured uncertainties of our most calculated orbital elements, we feel confident in the accuracy of our orbital elements. Our confidence in them is further bolstered by the low magnitude of uncertainties calculated for the right ascensions and declinations (*see Table 2*).

Since our methodology to achieving the goal is relatively simple and straight-forward, there are multiple areas to improve, primarily in the diversity of methods used to determine the orbital elements. While some alternatives were tested (*see Section 2.4*) such as contrasting accuracy of the truncated Taylor series to the closed form of f and g iteration, time constraints hindered our ability to test the differential correction method for orbital element uncertainties (currently using Jackknife method for calculating uncertainties of orbital elements) as well as the method of Laplace for determining orbital elements. Such comparisons could reduce potential errors introduced by using a singular, preliminary method.

However, there are other areas where errors are unavoidable and beyond our ability to eliminate. Defects in the chip could generate hot pixels that show up as white spots or lines as visible in few of our images that may interfere with the asteroid's visibility in the image (or in worst case scenarios, cover up the asteroid entirely). Dark current as well as electronics making up the telescope both consistently generate noise, irregardless of how we alter the telescope/camera settings. The noise is mitigated through the use of biases and darks in image reduction on CCDsoft as well as maintaining a low chip temperature. Still, we recommend lower chip temperatures in future repeats of this experiment, raising it only in order to keep a consistent temperature if lower temperatures overexert the cooler. Poor weather conditions have hindered our scheduled observations, resulting in slightly inconsistent time spans between each observation as well as interference in the asteroid visibility in the images taken in observation 3 (*noted in bottom of page 3*).

A. MPC Report

```
COD 719
CON A. W. Rengstorf
CON [adamwr@pnw.edu]
OBS A. Polish, M. Sere, L. Zhu
MEA A. Polish, M. Sere, L. Zhu
TEL 0.36-m f/11 reflector + CCD
NET NOMAD
BND V
NUM 6
ACK Team 1 - 1972 XA

01866         C2016 06 22.17038 13 36 41.27  12 02 21.5          16.5 V      719
01866         C2016 06 22.19722 13 36 40.32  12 01 52.3          16.5 V      719
01866         C2016 07 04.14828 13 32 24.21  08 24 16.0          16.5 V      719
01866         C2016 07 04.18339 13 32 23.84  08 23 36.4          16.5 V      719
01866         C2016 07 12.14648 13 32 05.34  05 54 15.3          16.7 V      719
01866         C2016 07 12.19855 13 32 05.55  05 53 15.9          16.6 V      719
```

B. Cloudy Night Experiments

B.1. Data Collection Strategy and Methotology

In order to test for the effect of time and CCD temperature on noise levels in dark and bias frames, we kept one constant while varying the others. 5 images were taken for each combination of time and temperature. Our time dependence test for noise levels in dark frames consisted of time variations, beginning with 5 seconds, with each subsequent test having double the duration of the previous. These frames were taken at a constant temperature of 22C. Our bias and dark temperature dependent tests spanned -5C to 22C, with intervals of 3C.

After taking images, we reduced the dark frames by the bias frames in order to isolate the effects caused by the dark current on the pixel count. The bias frames were left alone.

With these images, we wrote up a Python code analyzing the standard deviation for each set of 5 images. Using these 5 images per experiment, we were able to create four noise images, using the following combinations: 1 & 2, 2 & 3, 3 & 4 and 4 & 5. These four noise images consisted of the difference between respective pixel counts between the set of two images. Each pixel value in the noise images were then divided by the square root of 2 to obtain the noise values, leaving us with 4 noise images per data point. From these noise images, we calculated the average noise value per data point by finding the average of each pixel per set of four images. This value allows us to find the uncertainty in our measurements.

Using matplotlib in Python, we fit the results to graphs in order to correlate the results to a model with slope uncertainties.

B.2. Initial Assumptions

B.2.1. Dark Time Dependent

We expected dark pixel counts to scale linearly with time. Knowing that pixel counts accumulate with time as photos strike pixels in the CCD, we reasoned that the rate of photons striking a

specific pixel on the CCD would be constant, and thus the rate of increase of pixel counts as a function of time would be constant as well.

B.2.2. Dark Temperature Dependent

Knowing that atoms will climb to higher energy levels at a higher temperatures, we assumed that the pixel counts would increase with CCD temperature. Unlike time dependence however, we assumed that the relationship between pixel counts and temperature would have a positive concavity. We did not come to a consensus on whether this relationship would be quadratic or exponential, but we assumed one of the two would be true. This reasoning came from the way a CCD works. Since there a non-zero distance between the center of a CCD potential well and the conduction band, we assumed that as temperatures increased, the ratio of electrons that escaped into the conduction band would increase at an increasing rate.

B.2.3. Bias Temperature Dependent

Like the temperature dependent dark frames, we assumed that the relationship between bias noise levels and temperature would be increasing with a positive concavity. The reasoning for this assumption was the same as that used to reach an assumption for the temperature dependent dark frames.

B.3. Bias Temperature

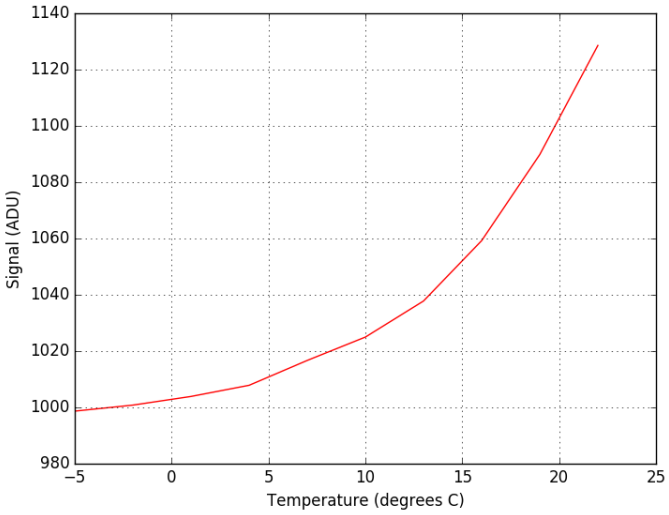

Figure 4: Bias levels as a function of temperature

According to the graph depicting the relationship between the signal and the temperature (4), there is a nonlinear relationship between the two elements. To consider bias frames as temperature dependent, the slope of the plotted graph will need to be closer to zero than the uncertainty of the slope. The uncertainty of the slope is calculated via plotting a line of best fit and calculating the deviations of the calculated graph's points from the line of best fit.

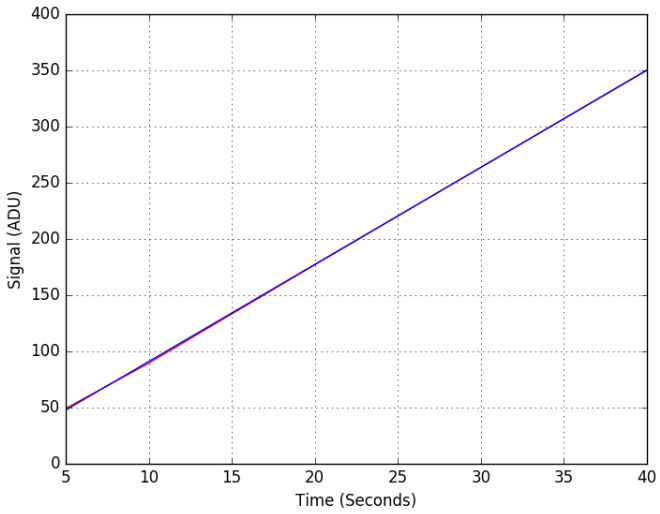

Figure 5: Dark current as a function of time

B.3.1. Dark Time Dependent

Using matplotlib on Python, we determined a linear relationship between the exposure time and signal. Visual inspection also yielded a consensus that the graph fits best to a linear function with slight deviations.

B.3.2. Dark Temperature Dependent

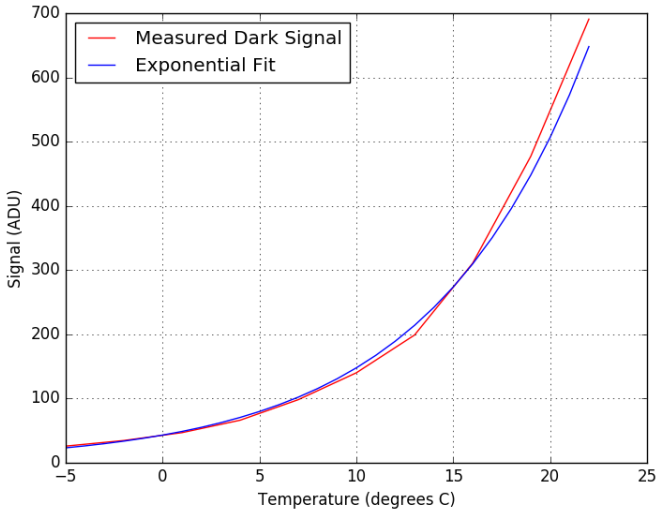

Figure 6: Dark current as a function of temperature

According to Figure 6, depicting the relationship between signal and temperature in dark frames, pixel counts increase non-linearly with temperature. Based on our observations, an exponential fit seems to describe the relationship fairly accurately. There is an apparent deviation between the plotted data and the fitted model, which may be due to a lack of data points or other outside factors,

but we can conclude that as temperature increases, the dark current increases at an increasing rate.

B.4. Conclusion

Our assumptions relating to the concavity of the graphed relationship between temperature and noise for bias and dark were confirmed as both graphs depict such aspect. Subsequently, our assumption on how the potential connection between the relationship and how the CCD functions is promoted. However, it was difficult to fit a linear or exponential function to some of the graphs, which points to a more complicated function that would require further investigation.

Given more opportunities to conduct cloudy night experiments, we could repeat the trials several more times to reinforce or refute our analysis and conclusion on the collected data. Further analysis on other aspects of the dark current and bias frames may refine our assumptions on the relationships based upon the new data yielded.